



Asymmetric Plasmonic Induced Ionic Noise in Metallic Nanopores

Journal:	<i>Nanoscale</i>
Manuscript ID	NR-ART-03-2016-001837.R1
Article Type:	Paper
Date Submitted by the Author:	18-Apr-2016
Complete List of Authors:	Li, Yi; IMEC, LST chen, chang; imec, Life Science Technology Willems, Kherim; IMEC, LST Lagae, Liesbet; IMEC, Groeseneken, Guido; Imec, Stakenborg, T; Interuniversitair Micro-Elektronica Centrum Van Dorpe, Pol; Imec, SSET



Journal Name

ARTICLE

Asymmetric Plasmonic Induced Ionic Noise in Metallic Nanopores

Yi Li,^{a,b,†} Chang Chen,^{a,c} Kherim Willems,^{d,a} Liesbet Lagae,^{a,c} Guido Groeseneken,^{a,b} Tim Stakenborg,^a and Pol Van Dorpe^{a,c}

Received 00th January 20xx,
Accepted 00th January 20xx

DOI: 10.1039/x0xx00000x

www.rsc.org/

We present distinct asymmetric plasmon-induced noise properties of ionic transport observed through gold coated nanopores. We thoroughly investigate the effects of bias voltage and laser illumination. We show that the potential drop across top-coated silicon nanocavity pores can give rise to a large noise asymmetry (~2-3 orders of magnitude). Varying the bias voltage has an appreciable effect on the noise density spectra, typically in the Lorentzian components. The laser power is found to strongly affect the ionic noise level as well as the voltage threshold for light-induced noise generation. The asymmetric noise phenomenon is attributed to plasmon-induced interfacial reactions which promote light-induced charge fluctuation into the ion flow and allow voltage modulation of photo-induced carriers surmounting over such Schottky junctions. This explanation was supported with the noise measurements of plasmonic nanopores. We further compared the ionic noise performances of gold nanocavities containing different material stacks, among which a thermal oxide passivation of the silicon successfully mitigates the light-induced noise and is also fully CMOS-compatible. The understanding of the described noise characteristics will help to foster multiple applications using related structures including plasmonic-based sensing or plasmon-induced catalysis such as water splitting or solar energy conversion devices.

Introduction

Solid-state nanopores have attracted a lot of interests for the analysis of the transport of nano-objects. Charged analytes can be electrophoretically dragged through such nanometre sized pores in a linear fashion.¹ The passage of these molecules can induce a transient fluctuation of the ionic current, the amplitude and duration time of which have been widely used to investigate single molecule events including DNA/RNA transport,² DNA-interaction,^{3,4} protein-receptor binding⁵ and viruses sensing.^{6–8}

Recently, plasmonic solid-state nanopores have been introduced to combine physical confinement of molecules, DC electric fields and intensive optical field intensities.^{9,10} Previously, the enhancement of highly confined electromagnetic field inside a nanopore has been utilized for localized heating,^{11,12} photoresistance switching,¹³ nanoscale trapping of nano-objects^{14,15} and highly-localized Raman spectroscopy of molecules.^{16,17} On the other hand, light

concentration in such plasmonic nanopores can influence ionic transport as well. For gold nanocavity pores, we have observed a strong increase of the ionic noise upon resonant plasmon excitation.¹⁸ The excess photo-induced noise intrinsic to plasmonic devices, limits both the accuracy of ionic measurement and sensitivity to the weak signals of translocation events.¹⁹ Having a consistent noise spectrum across nanopore devices and high signal-to-noise ratio upon laser illumination, are imperative for the development of nanopore systems.²⁰

In this paper, we investigate the noise properties in metallic nanopores upon resonant surface plasmon excitation. To the best of our knowledge, this is the first demonstration of an asymmetric photo-induced noise response through top-coated gold nanocavity pores. We show that the Lorentzian noise component can be modulated by the potential drop across the nanopore membrane, providing low-noise conditions below -0.6 V at low laser powers. Based on the asymmetry of the Lorentzian noise component, we show a means to mitigate the photo-induced noise using dielectric passivation in a single CMOS-compatible process.

Result and discussion

Our previous simulation and experimental work^{18,21} have known that resonant excitation of surface plasmons on this Fabry-Pérot nanopore structure can induce a strong additional noise component. The detail of nanopore fabrication is described in the Methods section. The ionic measurement scheme of such devices is depicted in Figure 1a. The chip

a. imec, Kapeldreef 75, Leuven, B3001, Belgium. Email: yi.li@imperial.ac.uk; pol.vandorpe@imec.be

b. Department of Electrical Engineering, KU Leuven, Kasteelpark Arenberg 10, 3001 Leuven, Belgium

c. Department of Physics and Astronomy, KU Leuven, Celestijnenlaan 200D, 3001 Leuven, Belgium

d. Department of Chemistry, KU Leuven, Celestijnenlaan 200G, 3001 Leuven, Belgium

† Electronic Supplementary Information (ESI) available: Numerical simulation of nanopore devices, Laser beam noise characterization and current noise dataset. See DOI: 10.1039/x0xx00000x

‡ Present address: Experimental Solid State Group, Department of Physics, Imperial College London, London, SW7 2AZ, U.K.

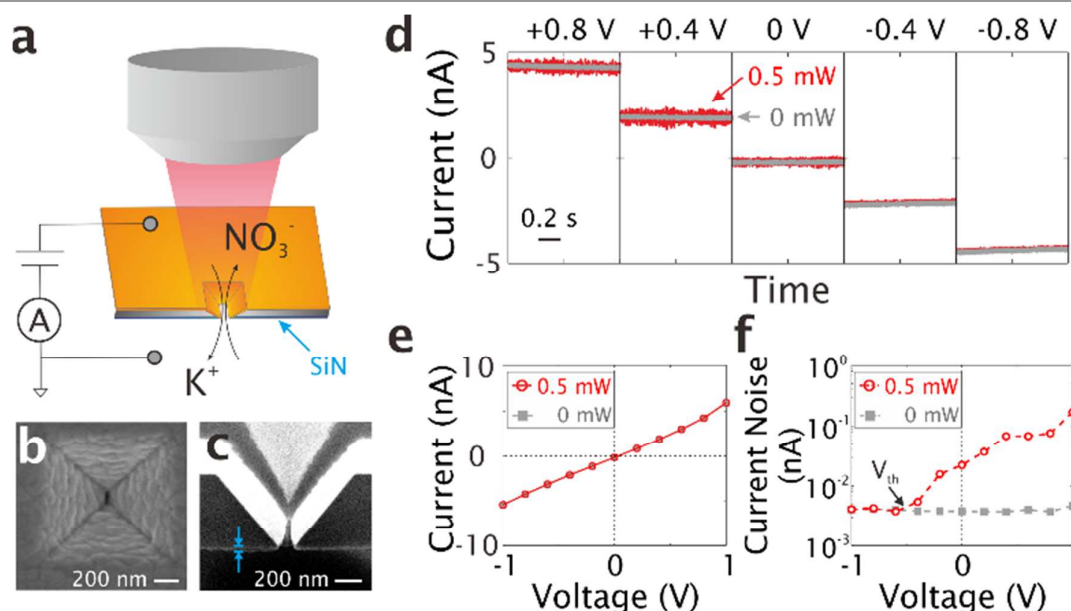


Figure 1. Ionic measurements of a plasmonic nanopore upon 785 nm laser illumination. (a) Schematic representation of the concept. Plasmon-induced effects are measured by means of ionic current flowing through the nanopore. (b) Top-view SEM image of a plasmonic nanocavity pore, which size is characterized as 13 nm × 98 nm. (c) Cross-section SEM image of the nanopore device. The blue arrows indicate the formation of SiN layer. (d) Measured temporal ionic current traces of 0 mW (grey) and 0.5 mW (red) at +0.8 V, +0.4 V, 0 V, -0.4 V and -0.8 V. (e) Current-voltage curves of panel (d) at 0 mW and 0.5 mW. (f) Natural logarithmic plot of the root-mean-square (RMS) current noise (between 50 Hz and 1 kHz). The red hollow circles stand for the values measured at 0.5 mW of 785 nm laser irradiation, while the grey squares for the control values without laser illumination. The black arrow indicates the threshold voltage, where the current noise is about to increase dramatically.

containing a through-wafer nanocavity is mounted into a custom-made flow cell to separate the electrolyte into two individual reservoirs. Since plasmonic excitation at different wavelengths has been investigated previously,¹⁸ we confine ourselves to use a 785 nm laser beam, tightly focused onto a gold nanopore with a typical size of 15 nm by 100 nm, verified by SEM in Figure 1b. Numerical simulation of such nanopore devices in the supporting information of Figure S1 confirms the resonance near the excitation at 785 nm wavelength. Figure 1c illustrates the cross-section SEM image of the nanopore, through which we can monitor the ion current flow upon laser illumination.

Figure 1d presents examples of current traces under laser illumination (red) and without laser illumination (grey), recorded from +0.8 V to -0.8 V. Upon switching on the laser, the current response shows a distinct current noise behaviour. Taking a laser illumination of 0.5 mW, the current noise increases dramatically at positive biases. In contrast, current noise in the dark condition remains stationary and does not respond to the bias voltage. To characterise the ionic current traces quantitatively, we plot the mean current and root-mean-square (RMS) current noise in Figure 1e and 1f. Figure

1e indicates a linear current-voltage (*I*-*V*) response, symmetric around 0 V, whereas a negligible change is observed upon 0.5 mW laser illumination. However, the noise RMS value (from Figure 1b), as illustrated in Figure 1f, reveals a strong voltage dependence. At 0.5 mW, the photo-induced excess noise increases with increasing bias voltage, once a threshold voltage (V_{th}) of -0.6 V is reached. Below -0.6 V, the current noise under laser illumination overlaps with the ones in the dark condition. This shows that plasmonic excitation exerts rare impacts on the current noise when being highly negative biased.

To understand the details of the noise properties as a function of bias voltage, we display the power spectral densities (PSD) of the noise in Figure 2. According to the experiments in the Supporting Information of Figure S2, we can eliminate the noise source generated by the laser beam. Moreover, Lorentzian components in Figure 2a-c are pronounced and exhibit consistent morphology to our previous report.¹⁸ The observed Lorentzian components scale with increasing laser power at 0.5 mW and 1.5 mW. As the bias changes from positive to negative, the Lorentzian components

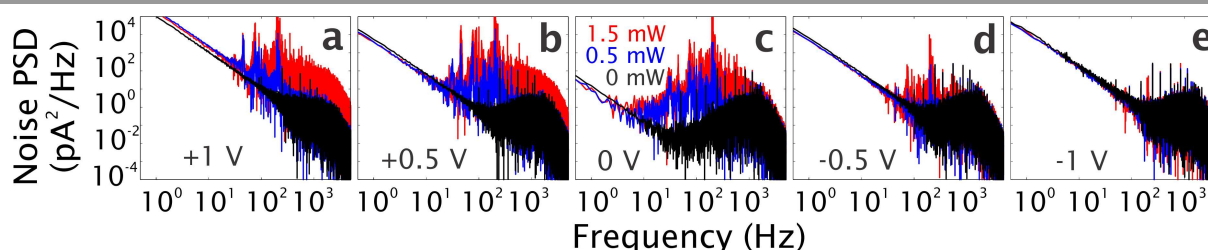


Figure 2. Noise power spectral densities (PSD) at different bias voltages. (a) +1 V; (b) +0.5 V; (c) 0 V; (d) -0.5 V and (e) -1 V. The black, blue and red curves indicate the PSD spectra at 0 mW, 0.5 mW and 1.5 mW. The low-pass filter is set at 2k Hz.

in Figure 2d,e gradually decrease and vanish at -1 V. We notice the low-frequency $1/f$ noise responses to the bias voltage but does not couple with the laser power. This $1/f$ noise component exists and shows good agreement with conventional Silicon Nitride (SiN) nanopores^{22,23} and ultra-thin graphene pores.²⁴ To separate the Lorentzian components from the $1/f$ noise, all RMS current noise measurements in this work have been processed with a band-pass filter between 50 Hz and 1 kHz.

Figure 3a illustrates the biased current noises as a function of laser power. At -1 V, no laser induced effect is observed and the amplitude of noise sets a baseline for the device noise level. Besides the current noise at -0.5 V, which could be considered to be a linear response to the laser power, all the measurements follow exponential growth, which parallels with the previously reported results.¹⁸ More detailed plots of the dataset are in Figure S3 of the Supporting Information. Figure 3b presents the threshold voltage V_{th} as a function of laser power, corresponding to a logarithmic decay close to -1 V.

To account for the observations of asymmetric ionic noise, we propose a photo-induced carrier process based on interfacial bond reactions. Figure 4a shows the process of the

ionic noise generation along with the interfacial reactions. Upon laser illumination, the plasmons can leak either directly to modes in silicon or through the path at the bottom of the gold cavity in contact with silicon. The excited electron-hole pairs in the silicon (dashed area in Figure 4a) are capable of semiconductor-mediated photocatalysis. We have previously ruled out the pathway for noise generation at gold-electrolyte interfaces which supports the idea that silicon-electrolyte boundaries is the source of noise,¹⁸ indicated by the noise activity occurs adjacent to the pore. Additionally, non-elevated mean current in Figure 1e excludes net light-induced charge transfer. Consequently, we list the probable half reactions with either electrons (I and II) or holes (III) processes. The combination of these processes could alter the surface charges and/or ion-ion fluctuations. Furthermore, the high device stability upon light illumination confirms that the plasmon-induced ionic noise processes are highly reversible. The noise generation does not consume the top gold layer, which is confirmed experimentally by observing stable size and conductance of our nanopores in the scale of a few hours. In addition, the silicon membrane does not exhibits changes in

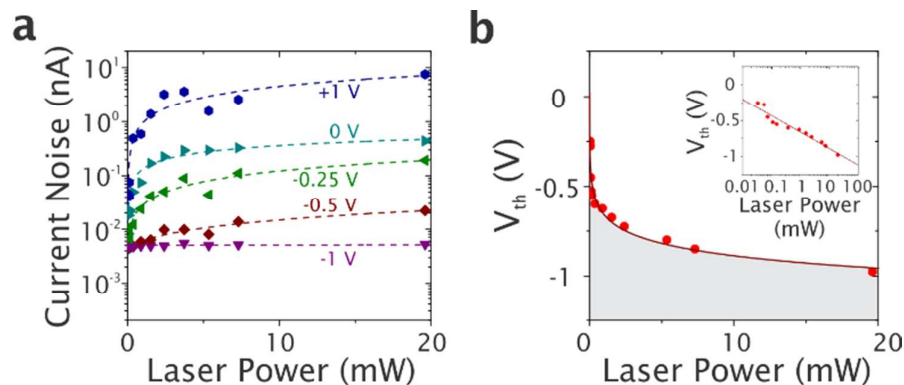


Figure 3. (a) Current noise (between 50 Hz and 1 kHz) as a function of laser power. (b) Voltage threshold V_{th} as a function of 785 nm laser power. The grey area under the curve indicate the conditions maintaining ground floor noise under laser illuminations. The inset is the natural logarithmic plot of panel b.

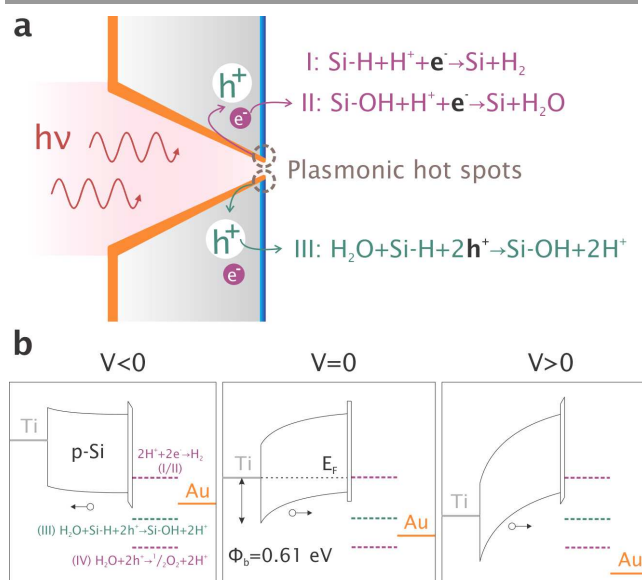


Figure 4. (a) Schematic of plasmonic induced ionic noise generation. (b) Proposed Energy band diagram of a Metal/p-Si/SiN/electrolyte junction. The Ti/p-Si Schottky barrier is about 0.61 eV. Photo-induced holes promote the fluctuations and reactions at the interfaces, which leads to the generation of ionic current noise.

thickness as the membrane area is more than 3 orders larger than the nanopore area ($1 \mu\text{m}^2$). We predict that photo-induced holes, as the majority carrier, promote the evolution of dangling bonds at the Si-electrolyte interface, which in turn produce the ionic noise in terms of surface bonds or charge fluctuations, as well as ion-ion correlations. The above-mentioned processes support our experimental observation, but does not yet fully describe the voltage dependence.

To elucidate the asymmetry of current noise, Figure 4b shows the energy band diagram of the device in the electrolytes. First, the generation of hydrogen gas has been experimentally confirmed when illuminated in water,^{25,26} although the production rate between hydrogen and oxygen is far more than two.²⁷ Second, the water related photo-catalytic process on a silicon surface may not be a complete water-splitting. Redox potentials of the two half-reactions for water-splitting are marked with two red dashed lines. To make the hydrolysis of water thermodynamically favourable, the band gap should be able to straddle these redox potentials. Due to the much higher potential required for O_2 evolution using Si, complete oxygen generation does not usually occur. This could be attributed to another half reaction that holds at a lower potential and can be spanned by the band gap of Silicon. Liu et al show that the production of hydrogen gas on the Si nanowires can occur through the cleavage of Si-H bonds and the formation of Si-OH bonds.²⁷ The work function of the process that reversibly forms Si-OH bonds is shown in Figure 4b as green dashed lines. This implies that the probability of generating oxygen gas could be prohibited by interfacial half-reaction of cleaving and forming surface bonds.²⁷

Schottky junction formation at the interface of Titanium and p-type Silicon plays a crucial role on the noise asymmetry. Interestingly, when illuminating the nanopores through the electrolyte, the excess holes in this device are likely to efficiently promote photo-catalysis.²⁸ At zero bias in Figure 4b, this Schottky barrier inhibits hole carrier injection to the metal. Thus, the transport of holes must occur at the other interface, leading to strong surface interactions with the electrolyte. When positive biases are applied, the barrier becomes more predominated, activating the surface reaction. At negative

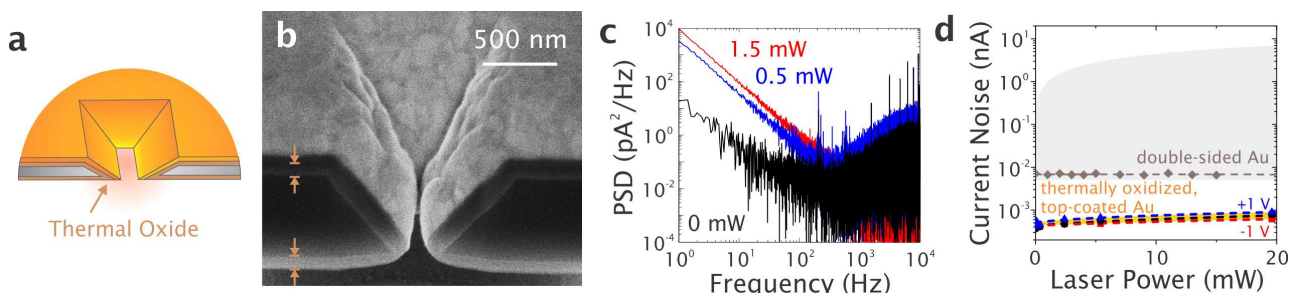


Figure 5. Thermally oxidized nanopores. (a) Schematic drawing of gold nanopore with thermal oxide at both sides of the silicon structure. (b) Cross-section SEM image of a gold coated nanopore device. The brown arrows indicate the ~ 77 nm thick of thermal oxide layers. The bar is 500 nm. (c) The noise power spectral densities of the device at 0 mW, 0.5 mW and 1.5 mW. The bias voltage is set at 0 V. (d) Current noise (between 50 Hz and 1 kHz) as a function of laser power. Blue triangles, black dots and red squares present the values of thermally oxidized chips for +1 V, 0 V and -1 V, which also defines the orange region for the noise levels. The results from double-sided gold nanopores are shown as brown diamonds, while the grey region presents the noise levels for top-coated gold nanopores.



Journal Name

ARTICLE

biases, photo-generated holes begin to have sufficient energy to cross the barrier and inject into the metal layer. Therefore, holes could neither reach the semiconductor-electrolyte interface nor promote interfacial interactions, which agrees with our observation of the noise reduction. Moreover, our finding of the threshold voltage value at ~ 0.6 V in Figure 3b is in a good agreement of the reported Ti/p-Si barrier height Φ_b of 0.61 eV.²⁹ This supports the idea that the Schottky barrier is the origin of noise asymmetry.

In order to further confirm the noise source at the silicon adjacent to the metal nanopores, we employ a process flow featuring thermal oxidation to passivate the devices with the best quality of silicon dioxide. Figure 5a presents a schematic diagram of the gold-coated thermally oxidized nanopores. The details of thermal oxidation and related processes are described in the Methods section. Thermal oxidation has unique ability to coat the both side with high quality silicon oxide, which have hitherto been instrumental to the industry's success.³⁰ A cross-section SEM image is given in Figure 5b, in which the thickness of thermal oxide is confirmed to be ~ 77 nm. Despite a slight red-shift of the optical resonance compared to the device in Figure 1, the plasmonic excitation of this device remains at approximately 785 nm wavelength.

The experimental results in Figure 5c show a distinct noise spectra upon plasmonic excitation. The Lorentzian noise components, which correspond to the interactions at the silicon/electrolyte interfaces, have been largely eliminated. This confirms that the high quality of the as-grown thermal oxide is able to block the transport of photo-induced carriers from Silicon to the surroundings. However, the observed $1/f$ noise manifests itself and increases upon laser illumination. The enhancement of $1/f$ noise could be attributed to light-induced surface charge effect but still remains poorly understood.³¹

Figure 5d summarizes the ionic noise performance of different metallic nanopore structures. Derived from the results in Figure 3a, the grey region defines the noise level in the range between -1 V and +1 V, providing a general case for gold-coated silicon nanocavity pores. As our previous work¹⁸ shows, double-sided gold nanopores are capable of the rejection of the plasmon-induced ionic noise. We plot the results from double-sided gold devices as well. The noise level of double sided gold nanopores is located at the bottom noise boundary of top-coated devices. The most surprising fact is that the noise level of thermally oxidized nanopores is more than one order of magnitude lower than the rest of gold nanopores.

Conclusions

The effect of laser excitation and varying bias voltage on the asymmetric noise properties of a plasmonic nanocavity pore has been investigated. To actively control the ionic noise upon laser irradiation, the interface between gold nanopore devices and dielectric materials has been used to eliminate unwanted noise source. While focusing the laser spot onto the gold nanocavity pores in the presence of the SiN beneath, voltage-dependent current noise is observed for the first time. Precluding the reported bias-dependent $1/f$ noise, the Lorentzian components in noise power densities are found to be modulated by the cross-membrane voltage. The observed noise above the threshold voltage can be attributed to the interfacial reaction, via defects, dangling bonds or pinholes through the SiN layer. By carefully analyzing the threshold voltages corresponding to different laser conditions, the operational conditions are located at negative biases with low laser powers, which pave the way for low-noise single-molecule optical nanopore applications.

Thermal oxidation of nanocavities has been investigated for the reduction of noise in these devices. These types of nanocavities coated with a gold layer, not only provide a much lower noise level without laser illumination, but also completely prevent the generation of Lorentzian components. This provides us a practical solution for the use of a single-step CMOS-compatible process to improve our device performance.

In addition to the goal of a low-noise nanopore biosensor, the demonstrated voltage dependency can further support various plasmon-induced catalysis. It is worth noting that, with increasing light illumination, the negative shift of threshold voltage indicates a co-operational process between the external potential and the generated photovoltaic potential, thus regulating photo-reduction.²⁸ Last but not the least, the noise measurements enable us to come up with a much more sensitive method to understand and characterize the photo-electrochemical process, rather than ionic flux based measurements.

Methods

Fabrication of Metallic Nanopores

The process of 200 mm wafer scale silicon nanocavity array fabrication was previously introduced.³² Nanocavity structures were defined by DUV lithography and followed by TMAH anisotropic etching. The wafer was then temporarily bonded to a carrier wafer and thinned down to 200 μm . Vertical fluidic channels with a diameter of 70 μm were opened by deep reactive ion etching (DRIE) for 90 min. Then both the device

and the carrier wafer were together diced into 21×21 mm² pieces. We then separated the thinned devices containing single cavity arrays from the carrier substrate by heating at 90 °C on a hot plate then removed the top bonding polymer HT10.10 (Brewer Science Inc.) by RCA-1 cleaning. The silicon nanocavities were completed by performing vapour hydrogen fluoride (VHF) etching for 35 min to completely remove the buried oxide layer.

For SiN passivated nanopores, a 50 nm SiN layer was deposited on the backside by plasma enhanced CVD at 350 °C and followed by sputtering 10 nm of Ti and 200 nm of Au on the top surface of the cavities.

For thermally oxidized nanopores, silicon nanocavity arrays were first rinsed by RCA-2 cleaning to remove metallic contaminants. Then, dry oxidation was performed using the HiTech benchtop furnace for 2 hours. A 77 nm oxide layer was formed on both sides of the nanocavities (Figure 4b). Finally, a layer of 10 nm Ti and 200 nm Au was sputtered on top of the cavities.

Experimental Setup

The chip containing a through-wafer nanocavity was rinsed with acetone, isopropanol and ethanol, and further dried with N₂ gas. Then, the chip was glued with Kwik-Cast (World Precision Instrument) on a polyacrylamide substrate, which has a 3 mm diameter hole at the centre. To clean the chip-substrate, a 1 min O₂ plasma treatment was performed on each side. The chip/substrate was mounted into a custom-made PMMA optical flow cell to separate the electrolyte into two individual reservoirs. A buffer solution (10 mM KNO₃, 10 mM Tris-acetate, and 1 mM EDTA, pH 8.0) was used during all measurements. Freshly prepared Ag/AgCl electrodes were placed at 1 cm away from the lens. It is worth noting that chloride-based solution could change permanently in our experiments. The use of Ag/AgCl in KNO₃ buffer solution practically supports a (quasi-)stable potential on the time scale of hours without size/conductance changes. Using a resistive feedback amplifier ($\beta = 0.1$, Axopatch 200B), ionic current traces were recorded at 100 kHz bandwidth with 250 kHz sampling rate. A 60× water immersion lens (Olympus, NA 0.9) was dipped into the top reservoir. An incident laser at 785 nm wavelength was focused on the nanocavity with its polarization initially perpendicular to the longitudinal axis of the structure. The diameter of the laser spot was estimated as ~1 μ m. RMS current noises were calculated with 0.1 s traces.

Acknowledgements

We thank Jos Moonens and Josine Loo for e-beam assistance, Dr. Tiannan Guan, Dr. Frederik Ceysens and Prof. Robert Puers for the help on thermal oxidation, MSc. Yiming Yang for the assistance of FIB sample preparation and Brock Doiron for critical reading of the manuscript and linguistic help.

Notes and references

- 1 C. Dekker, *Nat. Nanotechnol.*, 2007, **2**, 209–15.
- 2 M. Van Den Hout, G. M. Skinner, S. Klijnhout, V. Krudde and N. H. Dekker, *Small*, 2011, **7**, 2217–2224.
- 3 H. Chang, F. Kosari, G. Andreadakis, M. A. Alam, G. Vasmatzis and R. Bashir, *Nano Lett.*, 2004, **4**, 1551–1556.
- 4 Z. Liang, Z. Tang, J. Li, R. Hu, D. Yu and Q. Zhao, *Nanoscale*, 2015, **7**, 10752–10759.
- 5 R. Wei, V. Gatterdam, R. Wieneke, R. Tampé and U. Rant, *Nat. Nanotechnol.*, 2012, **7**, 257–263.
- 6 R. W. DeBlois and C. P. Bean, *Rev. Sci. Instrum.*, 1970, **41**, 909–916.
- 7 A. McMullen, H. W. de Haan, J. X. Tang and D. Stein, *Nat. Commun.*, 2014, **5**, 4171.
- 8 S. Liu, Y. Zhao, J. W. Parks, D. W. Deamer, A. R. Hawkins and H. Schmidt, *Nano Lett.*, 2014, **14**, 4816–4820.
- 9 C. Chen, *Plasmonic nanopores for direct molecular identification*, 2011.
- 10 S. Pud, D. V. Verschuere, N. Vukovic, C. Plesa, M. P. Jonsson and C. Dekker, *Nano Lett.*, 2015, **15**, 7112–7117.
- 11 M. P. Jonsson and C. Dekker, *Nano Lett.*, 2013, **13**, 1029–1033.
- 12 C. R. Crick, P. Albella, B. Ng, A. P. Ivanov, T. Roschuk, M. P. Cecchini, F. Bresme, S. A. Maier and J. B. Edl, *Nano Lett.*, 2015, **15**, 553–559.
- 13 Y. Li, F. Nicoli, C. Chen, L. Lagae, G. Groeseneken, T. Stakenborg, H. W. Zandbergen, C. Dekker, P. Van Dorpe and M. P. Jonsson, *Nano Lett.*, 2015, **15**, 776–782.
- 14 C. Chen, M. L. Juan, Y. Li, G. Maes, G. Borghs, P. Van Dorpe and R. Quidant, *Nano Lett.*, 2012, **12**, 125–132.
- 15 S. Kerman, C. Chen, Y. Li, W. VanRoy, L. Lagae and P. Van Dorpe, *Nanoscale*, 2015, **7**, 18612–18618.
- 16 C. Chen, J. A. Hutchison, F. Clemente, R. Kox, H. Uji-I, J. Hofkens, L. Lagae, G. Maes, G. Borghs and P. Van Dorpe, *Angew. Chem. Int. Ed.*, 2009, **48**, 9932–9935.
- 17 C. Chen, J. A. Hutchison, P. Van Dorpe, R. Kox, I. De Vlaminck, H. Uji-I, J. Hofkens, L. Lagae, G. Maes and G. Borghs, *Small*, 2009, **5**, 2876–2882.
- 18 Y. Li, C. Chen, S. Kerman, P. Neutens, L. Lagae, G. Groeseneken, T. Stakenborg and P. Van Dorpe, *Nano Lett.*, 2013, **13**, 1724–1729.
- 19 J. K. Rosenstein, M. Wanunu, C. a Merchant, M. Drndic and K. L. Shepard, *Nat. Methods*, 2012, **9**, 487–492.
- 20 M. Zorkot, R. Golestanian and D. J. Bonthuis, *Nano Lett.*, 2016, Mar 15. Article ASAP
- 21 C. Chen, L. Lagae, G. Maes, G. Borghs and P. Van Dorpe, *Phys. Status Solidi - Rapid Res. Lett.*, 2010, **4**, 247–249.
- 22 R. M. M. Smeets, N. H. Dekker and C. Dekker, *Nanotechnology*, 2009, **20**, 095501.
- 23 C. Tasserit, A. Koutsioubas, D. Lairez, G. Zalczer and M. C. Clochard, *Phys. Rev. Lett.*, 2010, **105**, 260602.
- 24 S. J. Heerema, G. F. Schneider, M. Rozemuller, L. Vicarelli, H. W. Zandbergen and C. Dekker, *Nanotechnology*, 2015, **26**, 74001.
- 25 I. Oh, J. Kye and S. Hwang, *Nano Lett.*, 2012, **12**, 298–302.
- 26 C. Liu, J. Tang, H. M. Chen, B. Liu and P. Yang, *Nano Lett.*, 2013, **13**, 2989–2992.
- 27 D. Liu, L. Li, Y. Gao, C. Wang, J. Jiang and Y. Xiong, *Angew. Chem. Int. Ed.*, 2015, **127**, 3023–3028.
- 28 N. R. Mathews, P. J. Sebastian, X. Mathew and V. Agarwal, *Int. J.*

Journal Name

ARTICLE

Hydrogen Energy, 2003, **28**, 629–632.

29 M. O. Aboelfotoh and K. N. Tu, *Phys. Rev. B*, 1986, **34**, 2311.

30 A. I. Kingon, J.-P. Maria and S. K. Streiffer, *Nature*, 2000, **406**, 1032–1038.

31 N. Di Fiori, A. Squires, D. Bar, T. Gilboa, T. D. Moustakas and A. Meller, *Nat. Nanotechnol.*, 2013, **8**, 946–51.

32 K. Malachowski, R. Verbeeck, T. Dupont, C. Chen, Y. Li, S. Musa, T. Stakenborg, D. Sabuncuoglu Tezcan and P. Van Dorpe, *ECS Trans.*, 2013, **50**, 413–422.